NUCL SCI TECH (2019) 30:124
https://doi.org/10.1007/s41365-019-0641-z

Neutron penetration in labyrinths under different beam losses

Yao Yang[1,2] · Wu-Yuan Li[1] · You-Wu Su[1] · Wei-Wei Yan[1] · Wang Mao[1] · Yang Li[1] · Bo Yang[1,2] · Li-Jun Wang[1]

Received: 20 December 2018 / Revised: 14 April 2019 / Accepted: 17 April 2019 / Published online: 12 July 2019

Abstract Multiple analytical methods and Monte Carlo simulations were performed to evaluate neutron penetration in straight and curved labyrinths. Factors studied included variations in beam losses of off-axis point source, on-axis point source, and line source. For the straight labyrinth, it was found that the analytical expressions neglect the dose rate platform appearing at the bend of the labyrinth, and the agreement between analytical methods and Monte Carlo estimation was related to the type of neutron source term. For the curved labyrinth, the neutron attenuation length obtained under different conditions was nearly identical and appeared to be in quite good accord with the empirical formula calculation. Moreover, the neutron energy spectra along the centerline distance of the labyrinth were also analyzed. In the first leg, differences in beam loss led to variance in the distribution of spectra, while in the second and subsequent legs, the spectra were similar, where the main contributors were thermal neutrons. This work is valuable for practical design of the labyrinths in the accelerator facilities.

Keywords Neutron penetration · Labyrinth · Beam loss · Analytical method · Monte Carlo code

This work was supported by the National Key R&D Program of China (No. 2017YFC0107700).

✉ You-Wu Su
suyouwu@impcas.ac.cn

1 Institute of Modern Physics, Chinese Academy of Sciences, Lanzhou 730000, China

2 University of Chinese Academy of Sciences, Beijing 100049, China

1 Introduction

The labyrinth is an important part of the overall shielding of any accelerator facility. It provides the passage of power cables, cooling-water pipes, ventilation pipes, and also for accelerator workers and equipment [1, 2]. Usually, the maze is designed to be multi-legged, so that the leaked radiation can be reduced to the dose limit [3]. The point source is the one located at the degrader, extraction septum, beam dump, experimental terminal, etc. In addition, in beam transport lines and accelerator rings, the beam losses are uniformly distributed; thus, they are called the line sources. For high-energy accelerators, the neutron component is most significant in terms of its ability to penetrate the shield [1, 3, 4]. Hence, it is essential to evaluate the neutron penetration in labyrinths, together with different beam losses and maze structures.

Several analytical methods are summarized in this paper for easy reading. The universal transmission curves [1] and its developed parametric form [5], Tesch's formula [6], Cossairt's formula [7], as well as the Monte Carlo program FLUKA [8, 9] are adopted to calculate the neutron penetration in the labyrinths. The former has the characteristic of convenient and fast calculation, while the latter is more accurate and also more suitable for complex geometries. In this work, the off-axis point source, on-axis point source, and the line source are considered in the simulations. The penetration in both straight and curved labyrinths is discussed. Multiple analytical methods are used to estimate the penetration of neutrons through the labyrinths, and the results are compared with the calculations by the Monte Carlo code. Besides, the neutron energy spectra along the centerline distance of the labyrinth are also studied.

2 Analytical methods

2.1 Universal transmission curves

The universal transmission curves [1] (hereinafter referred to as UTC) depict the relationship between the neutron transmission factor T and the scaled centerline distance $d/A^{1/2}$, where d is the distance from the source and A is the cross-sectional area of the tunnel. For the first leg, the transmission factor was given using four radiation sources including the on-axis point source, off-axis point source, line source, and the plane source. For the second and subsequent legs, the average of various theoretical results, as well as the upper limit and lower limit from various individual calculations, is given.

2.2 Stevenson–Fassò method

Stevenson and Fassò [5] developed two empirical formulas to calculate the transmission factor T_1 and T_2 for the first and the second leg, respectively. The expressions were used for the case of an off-axis source and are given by

$$T_1 = 1/(1 + 2.5D^{1/2} + 0.17D^{1.7} + 0.79D^3) \quad (1)$$

and

$$T_2 = 1/[1 + 2.8D(1.57)^{D+2}], \quad (2)$$

where $D = d/A^{1/2}$, d is the distance from the source and A is the cross-sectional area of the labyrinth.

2.3 Tesch's formula

Tesch [6] developed two formulas to calculate the dose rate attenuations in multi-legged labyrinths. The expression for the first leg in the case of the mouth of maze is directly viewing the source (also called the on-axis source) is expressed by

$$H(r_1) = 2H_0(a)(a/r_1)^2, \quad (3)$$

and for second and subsequent legs,

$$H(r_i) = \left(\frac{e^{-r_i/0.45} + 0.022A_i^{1.3}e^{-r_i/2.35}}{1 + 0.022A_i^{1.3}}\right)H_{0i}, i > 1, \quad (4)$$

where $H(r_i)$ is the dose rate in the ith leg at a distance of $r_i, H_0(a)$ is the dose rate in the mouth of the first leg, H_{0i} is the dose rate in the mouth of the ith leg, a is the distance from mouth to the entrance of labyrinth, and A_i is the cross-sectional area of each leg. The Tesch's formula is commonly used for the labyrinths with typical dimensions of 2.0 m height and 1–1.5 m width.

2.4 Nakamura and Uwamino's formula

Nakamura and Uwamino's formula [10, 11] gives another expression to calculate the neutron dose rate attenuation in the legs; it assumes that the attenuation obeys a simple $1/r^2$ law as follows:

$$H(r) = 2H(a)(a/r)^2, \quad (5)$$

where $H(r)$ is the dose rate in the leg, $H(a)$ is the dose rate in the entrance, a is half of the narrower dimension of width or height, and r is the distance measured from the entrance.

2.5 Cossairt's formula

Cossairt [7] has given a factorized approximation formula to calculate the neutron attenuation in the labyrinth for an on-axis source. For the first leg, the neutron dose equivalent rate is given by

$$H_1(\delta_1) = H_0(R)\left(\frac{r_0}{r_0 + \delta_1}\right)^2, \quad (6)$$

where $H_0(R)$ is the dose rate at the mouth, and r_0 is the given fitting parameter with a value of 1.4. For the second and successive legs, the following expression can be used to evaluate the dose rate transmissions along the maze:

$$H_i(\delta_i) = H_{i-1}(\delta_{i-1})\left(\frac{e^{-\delta_i/a} + Ae^{-\delta_i/b} + Be^{-\delta_i/c}}{1 + A + B}\right)^2, \quad (7)$$

where δ_i is the distance in the ith leg and a, b, c, A, and B are all given fitting parameters with values of 0.17, 1.17, 5.25, 0.21, and 0.00147, respectively.

Sheu [12] estimated the neutron transmission in the three-legged maze of Taiwan photon source, wherein the beam loss occurs near the center of the maze entrance. The FLUKA code [8, 9]-calculated results were compared with those by the Tesch's [6] and Cossairt's [7] method. The overall agreement between the FLUKA and Cossairt's results was satisfactory, while the Tesch's prediction underestimated the dose rate in the second and third legs. Based on the results, Sheu fitted the FLUKA results, and the new parameters for Eqs. (6) and (7) were given as: $r_0 = 1.12, a = 0.19, b = 0.75, c = 6.48, A = 0.61$ and $B = 0.028$.

2.6 Mauro's method

Mauro [2] systematically studied the attenuation factor of neutrons in circular mazes with different cross-sectional areas. The results indicate that the empirical formulas cannot correctly describe the transmission curves for the point on-axis source. Thus, a new expression is developed based on the FLUKA simulated results:

$$T = (kA^{1/2})(d/A^{1/2})^{-2hA^{1/2}} \tag{8}$$

with the parameters k and h given by

$$k = k_1 A^{-k_2/2},\ h = h_1 A^{-h_2/2}, \tag{9}$$

where k_1, k_2, h_1 and h_2 are fitting parameters with values of 0.7787, 1.2728, 0.8304, and 0.7307, respectively. Moreover, according to the calculated results with different codes by Gollon and Awschalom [3] as well as the FLUKA results conducted by Mauro [2], the above formulas also can be used in non-circular labyrinths with the same cross-sectional area.

It should be noted that the above formulas are suitable only for straight labyrinths. Curved labyrinths, although not common, are also necessary for some special equipment that cannot transport via the straight bends. The neutron attenuation length λ in the curved mazes has been studied by Patterson and Thomas [13, 14]. It has been found that λ is a function of only the maze radius R, and can be expressed by

$$\lambda = 0.7R^{1/2}, \tag{10}$$

where R is the labyrinth radius in meters and suitable for $4\,\mathrm{m} < R < 40\,\mathrm{m}$. Thus, the dose rate $H(x)$ at any circumferential distance x through the labyrinth is given by

$$H(x) = H_0 \exp(-x/\lambda), \tag{11}$$

where x and λ are expressed in mutually consistent units.

3 Monte Carlo simulations

3.1 Neutron source term

All the simulations were conducted by the FLUKA code version 2011. 2x. 3 [8, 9]. The precision defaults were used, and the heavy-ion interactions were treated by the BME, DPMJET, and RQMD-2.4 models. The neutron ambient dose equivalent rate was obtained by using the fluence-to-dose conversion factors [15, 16]. The user routine source.f was used in case of the line source, where the lost ions were uniformly distributed along the beam line. The sampled ions can be defined using the position and direction sampling formula [17, 18] shown below.

$$\text{Position sampling}\begin{cases} x = R_0\cos(2\pi\xi_1) \\ y = R_0\sin(2\pi\xi_1) \\ z = z_1 + \xi_2(z_2 - z_1) \end{cases} \tag{12}$$

$$\text{Direction sampling}\begin{cases} u = \sin\theta_0\cos(2\pi\xi_1) \\ v = \sin\theta_0\sin(2\pi\xi_1)\ , \\ w = \cos\theta_0 \end{cases} \tag{13}$$

where the (x, y, z) and (u, v, w) are the position and the direction cosines of the particle, respectively, R_0 is the radius of a supposed cylindrical surface for sampled particles, ξ_1 and ξ_2 are the random numbers which are produced by the function FLRNDM, z_1 and z_2 are the length range of the beam pipe in z axis, and θ_0 is the emission angle of the ion in the unit of radian. A schematic view of the line source model is given in Fig. 1 [18]. In this work, R_0 was 9.999 99 cm, which was slightly smaller than the beam pipe (made of stainless steel) with a radius R_1 of 10 cm. The beam incident direction was the positive of the Z axis, and with the emission angle θ_0 in $2°\ (3.49066 \times 10^{-2}$ rad). A point source was placed at position C (see Fig. 2), directly in view of the mouth of the labyrinth, and was called the on-axis point source; it was called the off-axis point source like if placed at position A or B. Moreover, if the entrance of the maze was located in front of a point source, like position A, this was also called the off-axis point source for forward direction. Likewise, the source term at position B was called the off-axis point source for backward direction.

3.2 Labyrinth model

The typical uranium beam at 800 MeV/u in High Intensity heavy-ion Accelerator Facility (HIAF) [19, 20] was used for all the simulations. For the point loss, the thick copper target, 5 cm in radius and 10 cm in length, was used to produce the neutron source terms. The labyrinth models for different beam losses are given in Fig. 2. The accelerator tunnel was 4 m in width and 4.5 m in height, and both the straight and curved labyrinths were 1.5 m in width and 2.5 m in height. The length of the three legs in the straight labyrinth was 3 m, 5 m and 2 m, respectively. The centerline radius R was 4.25 m for the curved labyrinth. All materials defined in the simulations came from the FLUKA material library, e.g., concrete, with a density of 2.35 g/cm^3, and consisting of H (1%), C

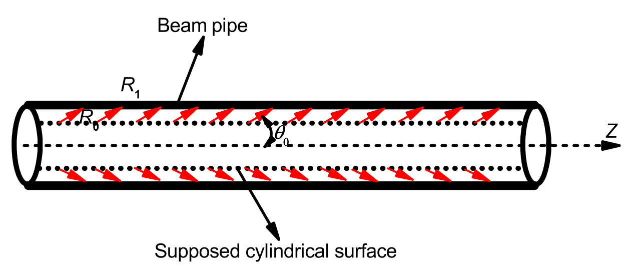

Fig. 1 (Color online) Schematic view of the line source model (not to scale)

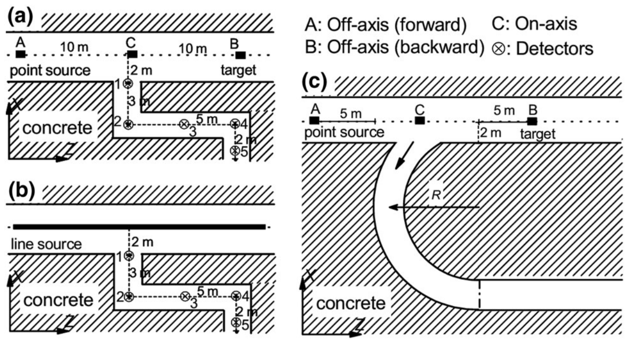

Fig. 2 The model of labyrinths for FLUKA simulations (not to scale). Five detectors, 1–5, were distributed along the maze. **a** The copper targets in position A, B and C are indicated, which represent the off-axis point source for forward, off-axis point source for backward, and on-axis point source, respectively. **b** Line source in the straight labyrinth. **c** Location of point sources in the curved labyrinth; the line source was also included (not shown here)

(0.1%), O (52.9107%), Na (1.6%), Mg (0.2%), Al (3.3872%), Si (33.7021%), K (1.3%), Ca (4.4%), and Fe(1.4%). Finally, an air-filled sphere detector having a radius of 40 cm was set at 5 positions (see Fig. 2); meanwhile, the USRBDX cards were employed to score the neutron energy spectra.

4 Results and discussion

4.1 Off-axis point source

The lethargy plotting of neutron energy spectra in forward and backward direction is illustrated in Fig. 3a, b, respectively. Both figures indicate that the spectra become softer with the increase in the distance from the entrance. The proportion of high-energy neutrons attenuates more rapidly by air and wall scattering, while thermal neutrons are dominated in the second and third legs. In other words, the high-energy neutrons are attenuated more easily than the low-energy ones. Besides, in Fig. 3a, a high neutron peak appears around 600 MeV; these neutrons are produced from the intranuclear cascade process and are focused mainly in the forward direction. Obviously, this phenomenon is a result of the fact that the entrance of labyrinth is located in the forward direction of the target. Furthermore, the high-energy neutrons can spread beyond the energy of projectile particles. This phenomenon can be interpreted as being high-momentum components of Fermi distribution [21]. In Fig. 3b, an evaporation neutron peak appears around 1 MeV; these neutrons are produced from the evaporation of the compound nucleus and can be described by the Maxwellian distribution.

Figure 4a, b compares the penetration curves calculated with analytical methods and the FLUKA simulations for forward and backward directions, respectively. Similar results are obtained as illustrated in these two figures. In the first leg, good agreement is observed between the Nakamura–Uwamino estimated curves and FLUKA simulations, while the UTC method and Stevenson–Fassò method lead to overestimation of about three to five times

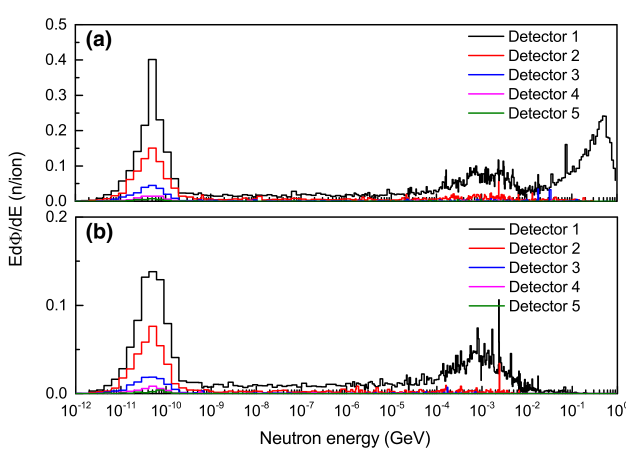

Fig. 3 (Color online) Lethargy plotting of neutron energy spectra at five detectors. **a** Off-axis point source for forward direction. **b** Off-axis point source for backward direction

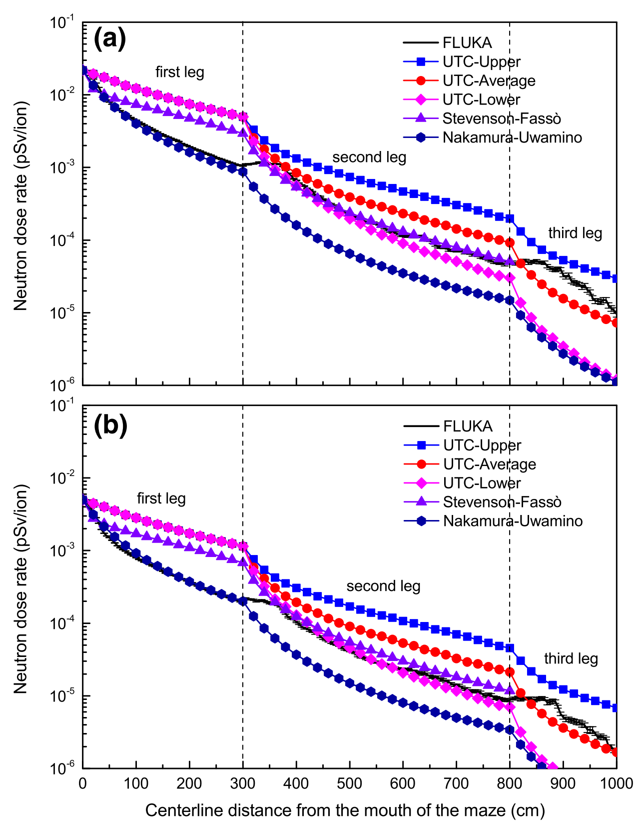

Fig. 4 (Color online) Neutron dose rate distributions along the centerline distance from FLUKA calculations and analytical methods. **a** Off-axis point source for forward direction. **b** Off-axis point source for backward direction

of the dose rate. Then, in the second leg, it is found that both the Stevenson–Fassò method and the lower limit of UTC curves are applicable to evaluate the neutron streaming in the labyrinth. Besides, in the third leg, the average value of UTC method is generally consistent with the FLUKA estimations. Finally, the dose rate platform at the bend of the labyrinth is almost neglected in empirical approaches.

4.2 On-axis point source

Figure 5 plots the dose rate penetrations from the on-axis point source. In the first leg, the UTC method-calculated curves show quite good agreement with the FLUKA code. However, the curves obtained by Tesch's and Mauro's methods are larger than the simulations; this is due to the short distance from the source, causing the transmission factor T to be greater than one [see in Eqs. (3) and (8)]. In the second leg, the analytical methods neglect the dose rate platform, as discussed above. However, as the distance increases, the results from Tesch's and the UTC-average methods become in good agreement with the Monte Carlo evaluations. At the end of second leg, the dose rate shows a slight increase, which can be explained by the contribution of the scattered neutrons. In the third leg, the UTC upper meets with FLUKA calculations within a factor of two.

In particular, in order to compare the penetration curves in the first leg obtained by multiple methods, the distance is increased to 10 m, and the results are indicated in Fig. 6. As presented, when $d < 4\,\mathrm{m}$ ($d/A^{1/2} < 2$), the UTC methods show good agreement, while when $d > 4\,\mathrm{m}$, the Mauro's approach is consistent with those of the FLUKA curves. Thus, the transmission of neutrons through a single leg from on-axis point source can be evaluated by the UTC methods when $d/A^{1/2} < 2$, and Mauro's method when $d/A^{1/2} > 2$.

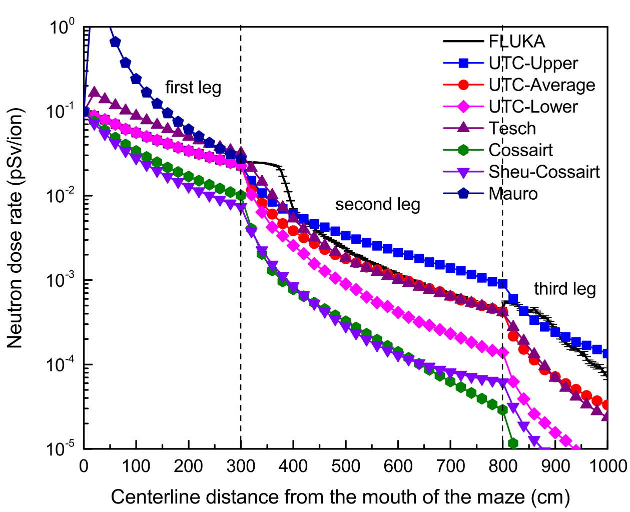

Fig. 5 (Color online) Neutron dose rate distributions from the on-axis point source predicted by the FLUKA code and analytical methods

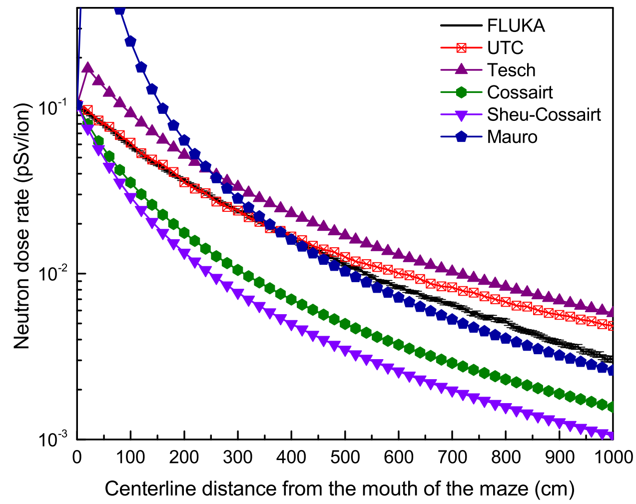

Fig. 6 (Color online) Neutron dose rate distributions through a single-leg labyrinth from on-axis point source calculated by the FLUKA code and analytical methods

4.3 Line source

The neutron energy spectra from on-axis point source and line source are indicated in Fig. 7a, b, respectively. The evaporation neutron peak still exists and is observed in the second detector from on-axis point source as indicated in Fig. 7a. This is due to the entrance of labyrinth being in direct view of the target. The emitted neutrons in 90° direction mainly come from the evaporation process of the compound nucleus, while for the line source, the thermal neutron peak, the evaporation neutron peak, and also the high-energy neutron peak are simultaneously observed in

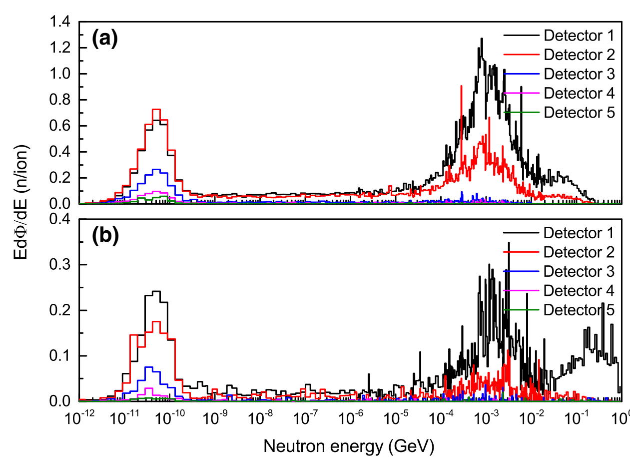

Fig. 7 (Color online) Lethargy plotting of neutron energy spectra for the five detectors. **a** On-axis point source. **b** Line source

the first detector. This occurs as a result of the line source being considered to be composed of multiple continuous point sources.

Figure 8 gives the neutron dose rate transmission curves from the line source. In the first leg, the Cossairt's model gives roughly consistent values with the FLUKA simulations. In the second leg, the UTC-average values and the Tesch's expression show quite good agreement. However, in the entrance of the third leg, no good matching curves appear. As the distance increases, the UTC upper curves agree with the FLUKA estimations within a factor of two.

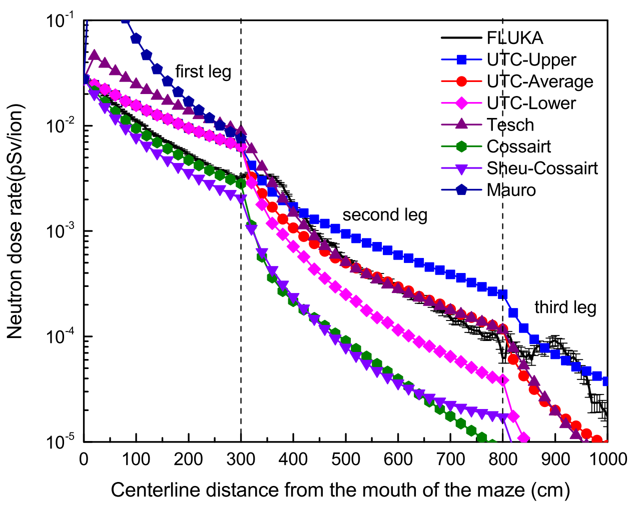

Fig. 8 (Color online) Neutron dose rate distributions from the line source evaluated by the FLUKA code and analytical methods

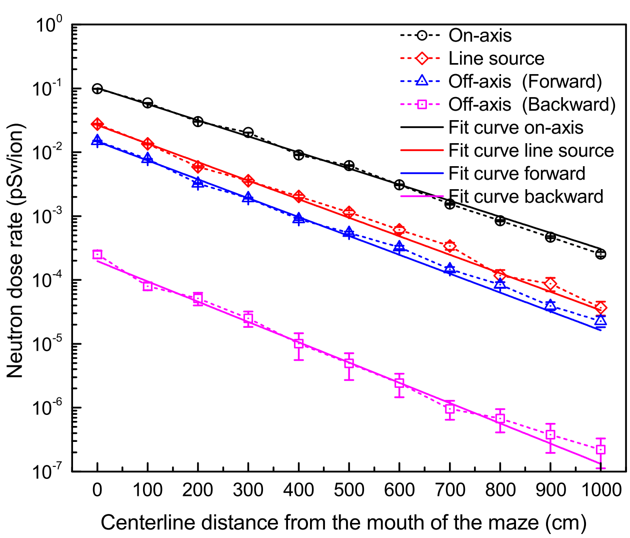

Fig. 9 (Color online) Neutron transmission curves for the curved labyrinth as a function of centerline distance from the mouth

4.4 Penetrations in curved labyrinth

In the case of the curved labyrinth, the neutron attenuation curves for different beam losses are shown in Fig. 9. It was found that the attenuation of the logarithm value of the dose rate is almost linear with distance. The neutron attenuation length λ determined by fitting the results and the coefficient of determination R^2 for different beam losses are given in Table 1. The comparison between the calculated and the fitted results appears to be quite good. The fitted λ values for different beam losses are almost consistent with the empirical formula calculation for $\lambda = 0.7R^{1/2} = 1.44\,\mathrm{m}$. Moreover, in case of the on-axis point source, the λ is about a factor of 1.2 larger than the empirical formula estimation. Thus, in the practical design, adding a factor of 1.5 is recommended to obtain a conservative estimation of the attenuation length.

5 Summary

This work investigated neutron penetration through the labyrinths. The obtained results from analytical approaches were compared with the Monte Carlo calculations for different beam losses and maze structures. The results of neutron spectra indicate that in the first leg, the diversity in beam losses leads to different distribution in spectra. However, in the second and subsequent legs, the proportion of thermal neutrons increased due to slowing down of the high-energy neutrons. For neutron transmissions, the following conclusions can be given:

For the straight labyrinths: (1) In the first leg, neutron attenuations were related to the energy spectra, and the analytical methods were suitable for specific beam loss. For example, for an off-axis point source, the $1/r^2$ law gives good agreement with the FLUKA calculations. For an on-axis point source, the universal transmission curves were applicable when $d/A^{1/2} < 2$, while for $d/A^{1/2} > 2$, the Mauro's method was recommended. Moreover, for a line source, the Cossairt's method gives roughly consistent values with FLUKA simulations. (2) In the second and subsequent legs, thermal neutrons were the main

Table 1 Fitted results of the attenuation length λ and coefficient of determination R^2 for different beam losses

	Off-axis (forward)	Off-axis (backward)	On-axis	Line source
λ	1.47	1.37	1.72	1.50
R^2	0.992	0.959	0.996	0.993

contributors to the radiation fields. Therefore, the neutron penetration shows the same phenomenon under different beam losses. The universal transmission curves were applicable for this situation.

For the curved labyrinths, the neutron attenuation length λ values were expected to be the same for different beam losses and show good agreement with the empirical formula calculation. Consequently, in the design of the curved labyrinths, the empirical formula can be used for fast calculations. Besides, adding a factor of 1.5 was recommended for a conservative estimation of λ for the on-axis point source.

References

1. National Council on Radiation Protection and Measurements. *Radiation Protection for Particle Accelerator Facilities*, NCRP report No 144 (Maryland, 2003), p. 255
2. E. Mauro, M. Silari, Attenuation of neutrons through ducts and labyrinths. Nucl. Instrum. Methods A **608**, 28–36 (2009). https://doi.org/10.1016/j.nima.2009.06.045
3. P.J. Gollon, M. Awschalom, Design of penetrations in hadron shields. IEEE Trans. Nucl. Sci. **NS18**, 741–745 (1971). https://doi.org/10.1109/TNS.1971.4326169
4. P.K. Sarkar, Neutron dosimetry in the particle accelerator environment. Radiat. Meas. **45**, 1476–1483 (2010). https://doi.org/10.1016/j.radmeas.2010.07.001
5. G.R. Stevenson, A. Fassò, *A Comparison of a Morse Calculation of Attenuation in a Concrete-Lined Duct with Experimental Data from the CERN SPS*, CERN Divisional Report TIS-RP/185/CF (1987)
6. K. Tesch, The attenuation of the neutron dose equivalent in a labyrinth through an accelerator shield. Part. Accel. **12**, 169–175 (1982)
7. J.D. Cossairt, *Approximate Technique for Estimating Labyrinth Attenuation of Accelerator-Produced Neutrons*, Radiation Physics Note No. 118 (Fermi National Accelerator Laboratory, Batavia, 1995)
8. T.T. Böhlen, F. Cerutti, M.P.W. Chin et al., The FLUKA code: developments and challenges for high energy and medical applications. Nucl. Data Sheets **120**, 211–214 (2014). https://doi.org/10.1016/j.nds.2014.07.049
9. A. Ferrari, P.R. Sala, A. Fassò, et al., FLUKA: a multi-particle transport code, CERN-2005-10 (2005), INFN/TC_05/11, SLAC-R-773
10. T. Nakamura, Y. Uwamino, Radioisotopes **35**, 51–56 (1986). **(in Japanese)**
11. Y. Uwamino, T. Nakamura, T. Okhubo et al., Measurement and calculation of neutron leakage from a medical electron accelerator. Med. Phys. **13**, 374–384 (1986). https://doi.org/10.1118/1.595879
12. R.J. Sheu, J. Liu, Investigation of radiation streaming and labyrinth design for the Taiwan Photon Source. Health Phys. **98**, 565–573 (2010). https://doi.org/10.1097/HP.0b013e3181c20e09
13. H.W. Patterson, R.H. Thomas, *Accelerator Health Physics* (Elsevier, Amsterdam, 1973), p. 451. https://doi.org/10.1016/B978-0-12-547150-3.X5001-4
14. J.D. Cossairt, *Radiation Physics for Personnel and Environmental Protection*, Fermilab Report TM-1834, Revision 15 (2016), pp. 139–140
15. International Commission on Radiological Protection, *Conversion Coeffcients for Use in Radiological Protection Against External Radiation*. ICRP Publication 74 (1997)
16. M. Pelliccioni, Overview of fluence-to-effective dose and auence-to-ambient dose equivalent conversion coefacients for high energy radiation calculated using the FLUKA code. Radiat. Prot. Dosim. **88**, 279–297 (2000). https://doi.org/10.1093/oxfordjournals.rpd.a033046
17. Q.B. Wu, Q.B. Wang, J.M. Wu et al., Study on induced radioactivity of China Spallation Neutron Source. Chin. Phys. C **35**, 596–602 (2011). https://doi.org/10.1088/1674-1137/35/6/017
18. C. Xu, Z.J. Ma, H.Y. Shi et al., The realization and verification of integrated modeling of the losing source items by using FLUKA for ERL-FEL. Nucl. Tech. **39**, 070503 (2016). https://doi.org/10.11889/j.0253-3219.2016.hjs.39.070503. **(in Chinese)**
19. Y. Yang, Y.W. Su, W.Y. Li et al., Evaluation of radiation environment in the target area of fragment separator HFRS at HIAF. Nucl. Sci. Tech. **29**, 147 (2018). https://doi.org/10.1007/s41365-018-0479-9
20. S. Ruan, J.C. Yang, J.Q. Zhang et al., Design of extraction system in BRing at HIAF. Nucl. Instrum. Methods A **892**, 53–58 (2018). https://doi.org/10.1016/j.nima.2018.02.052
21. D. Satoh, T. Kurosawa, T. Sato et al., Reevaluation of secondary neutron spectra from thick targets upon heavy-ion bombardment. Nucl. Instrum. Methods A **583**, 507–515 (2007). https://doi.org/10.1016/j.nima.2007.09.023